Journal of Quantitative Spectroscopy & Radiative Transfer 272 (2021) 107757

Contents lists available at ScienceDirect

Journal of Quantitative Spectroscopy & Radiative Transfer

journal homepage: www.elsevier.com/locate/jqsrt

Electromagnetic wave scattering by charged coated spheres

Chenxu Gao[a,b], Bingqiang Sun[a,b,*], Yijun Zhang[a,b]

[a] Department of Atmospheric and Oceanic Sciences & Institutes of Atmospheric Sciences, Fudan University, Shanghai 200438, China
[b] Innovation Center of Ocean and Atmosphere System, Zhuhai Fudan Innovation Research Institute, Zhuhai 518057, China

ARTICLE INFO

Article history:
Received 29 December 2020
Revised 16 May 2021
Accepted 17 May 2021
Available online 24 May 2021

Keywords:
Electromagnetic scattering
Charged coated spheres
Rayleigh approximation

ABSTRACT

Scattering characteristics of electromagnetic waves are analyzed by a uniformly charged coated sphere using the Lorenz–Mie theory. Numerical calculations are presented for charges on the surfaces of the interior core and exterior shell, respectively. When the surfaces are charged, the extinction efficiencies are affected by the radius ratio of the two layers and the surface potential. The scattering characteristics are further simplified to Rayleigh scattering using the Taylor expansion in a regime where scattering is significantly influenced by charges. The Rayleigh scattering in this regime can replace the analytical solution derived from the Lorenz-Mie theory.

1. Introduction

The scattering and absorption of electromagnetic waves by small particles have been intensively studied since the Lorenz–Mie theory was established [1-4]. The first exact scattering solution by a homogeneous coated sphere was proposed in the 1950s by Aden and Kerker [5], and discussed in detail by Bohren and Huffman [6]. Scattering by neutral spheres has also been examined in numerous studies [3-7]. However, atmospheric particles often possess charges generated by friction, atmospheric circulation, cloud charging, spray electrification, solid–solid contact, and gas ionization processes [8,9]. The net surface charges are vital for predicting lightning threats and tracking in remote-sensing [10,11]. In fact, several studies have investigated the charge generation mechanism associated with thunderstorms and electron collection by dust particles [12-15]. For example, the induction electrification process relies on pellet polarization by an electric field [16], while riming electrification is generally accepted for the primary noninductive charging process [17]. In this process, H^+ ions diffuse faster into the colder parts than OH^- ions under a temperature gradient; consequently, the melting ice particles are characterized by positively charged inner cores and negatively charged outer shells [18,19]. Moreover, the charging effect of coated dust particles with different chemical components has been studied, and extinction resonance peaks have been found due to the core-coat structure [15].

Numerous studies have highlighted the importance of charged particles on the scattering of electromagnetic waves. Bohren and Hunt [20] introduced the surface conductivity of an excess charge, which is position-independent and frequency-dependent, providing a classical equation for the motion of charges while assuming the presence of free excess surface charges. Further, Klačka and Kocifaj specified boundary conditions and presented numerical experiments for charged cosmic dust particles, water droplets, and ice grains in the Earth's atmosphere [21]. These authors also discussed the attenuation rates using classical and quantum physics [22] and refined the conductivity model [23]. Most studies of charged scattering effects use the above approach, focusing on intraband effects also known as free-electron effects [24]. There are also studies that reflect the effect of electrons in the change of refractive index [15,25]. According to these previous studies, the optical properties of particles with size parameters less than 10^{-3} exhibit remarkable differences between the charged and electrically neutral states, when the imaginary parts of the refractive indexes of these particles are sufficiently small [21-23,26]. For a particle significantly smaller than the incident wavelength, the first term of the analytical Lorenz–Mie solution dominates, with the corresponding theory termed as Rayleigh scattering or approximation [6,27]. The Rayleigh approximation, however, is considered inadequate for modeling scattering by small, charged particles, as the expansion coefficients a_n is scaled by the surface conductivity, which predetermines a mode of vibration [23,28,29].

Atmospheric particles are commonly complex in shape, mostly inhomogeneous, and multilayered; for example, melting graupel pellets [18] and slightly soluble aerosols [30]. Initial studies on scattering by multilayer particles used a two concentric sphere model [5], which were followed by generalization to the multilayer sphere [7,31-35]. The application of the discrete dipole approximation (DDA) method for the calculation of the charged effects

* Corresponding author at: Department of Atmospheric and Oceanic Sciences & Institute of Atmospheric Sciences, Fudan University, Shanghai 200438, China.
E-mail address: bingqsun@fudan.edu.cn (B. Sun).

https://doi.org/10.1016/j.jqsrt.2021.107757
0022-4073/

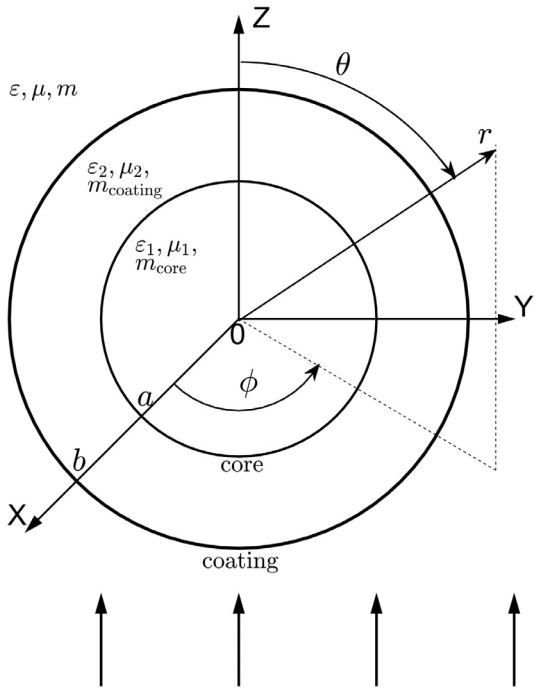

Fig. 1. Physical model for a charged coated sphere, where permittivity is square of refractive index.

of non-spherical particles has also been proposed recently [36]. Nonetheless, the optical response differences between charged and electrically neutral multilayer spheres have rarely been examined. By assuming that electrons are confined to the outer surface of a multilayer sphere, Li [37] reported that the effect of surplus charges on optical properties depends on the properties of the distributed charges, with the particle structures changing the extinction value but not the variation characteristics.

To elucidate the influences of the surface charges and complex structures of atmospheric particles, the characteristics related to scattering by a coated sphere with arbitrary free charges on the surfaces of the interior core or/and exterior coating are analytically derived using the Lorenz–Mie theory. In addition, a generalized model involving different charges on the surfaces is discussed based on core-shell structure aerosols. Most importantly, the Taylor expansion is applied to the analytical solution under a regime characterized by noticeable influences of surface charges. This study demonstrates that scattering by a charged coated sphere in that regime can be described using the Rayleigh approximation. In addition, calculating the scattering properties associated with the size parameter becomes easier because the size parameter is explicitly displayed in the Rayleigh approximation.

2. Generalized model

For a generalized model considering a charged coated sphere, charges are uniformly distributed along the core surface and the coating surfaces. The subscripts $n = 1$ and 2 denote the core and coating in this study, respectively, while the terms without the subscripts represent the surrounding medium. Further, the inner radius and outer radius of the coated sphere are a and b, respectively. For the core, coating, and surrounding medium, different permittivity, and permeability values are assumed for each region, as shown in Fig. 1.

2.1. Fundamental equations

For charged particle scattering, the fundamental equations for a time-harmonic electromagnetic field (E, H) must satisfy the Helmholtz equation as

$$\begin{cases} \nabla^2 E + k_n^2 E = 0, \\ \nabla^2 H + k_n^2 H = 0, \end{cases} \tag{1}$$

where $k_n^2 = \omega^2 \varepsilon_n \mu_n$, $n = 1, 2$, k denotes the wavenumber, ω is the angular frequency, while ε and μ are permittivity and permeability, respectively. An incident plane wave with an x-polarized electric field component can be written as [6]

$$E_i = E_0 e^{ikr\cos\theta} \hat{e}_x, \tag{2}$$

where E_0 is the amplitude of the incident electric field and the polarization direction in the spherical coordinates is expressed as

$$\hat{e}_x = sin\theta cos\phi \hat{e}_r + cos\theta cos\phi \hat{e}_\theta - sin\phi \hat{e}_\phi \ . \tag{3}$$

The divergence-free electromagnetic fields satisfying the Helmholtz equation can be expanded using the vector spherical harmonics as

$$\begin{cases} E_i = \sum_{n=1}^{\infty} E_n (M_{o1n}^{(1)} - iN_{e1n}^{(1)}), \\ H_i = \frac{-k}{\omega\mu} \sum_{n=1}^{\infty} E_n (M_{e1n}^{(1)} + iN_{o1n}^{(1)}), \end{cases} \tag{4}$$

$$\begin{cases} E_s = \sum_{n=1}^{\infty} E_n (-b_n M_{o1n}^{(3)} + ia_n N_{e1n}^{(3)}), \\ H_s = \frac{k}{\omega\mu} \sum_{n=1}^{\infty} E_n (a_n M_{e1n}^{(3)} + ib_n N_{o1n}^{(3)}), \end{cases} \tag{5}$$

$$\begin{cases} E_1 = \sum_{n=1}^{\infty} E_n \left(c_n M_{o1n}^{(1)} - id_n N_{e1n}^{(1)}\right), \\ H_1 = \frac{-k_1}{\omega\mu_1} \sum_{n=1}^{\infty} E_n \left(d_n M_{e1n}^{(1)} + ic_n N_{o1n}^{(1)}\right), \end{cases} \tag{6}$$

$$\begin{cases} E_2 = \sum_{n=1}^{\infty} E_n (f_n M_{o1n}^{(1)} - ig_n N_{e1n}^{(1)} + v_n M_{o1n}^{(2)} - iw_n N_{e1n}^{(2)}), \\ H_2 = \frac{-k_2}{\omega\mu_2} \sum_{n=1}^{\infty} E_n (g_n M_{e1n}^{(1)} + if_n N_{o1n}^{(1)} + w_n M_{e1n}^{(2)} + iv_n N_{o1n}^{(2)}), \end{cases} \tag{7}$$

$$E_n = i^n E_0 \frac{(2n+1)}{n(n+1)}, \tag{8}$$

where a_n, b_n, c_n, d_n, f_n, g_n, v_n, and w_n are expansion coefficients, with exp ($-i\omega t$)being suppressed in this study. The vector spherical harmonics M and N in Eqs. (4)–(7) are provided by Bohren and Huffman [6], and rewritten here as

$$M_{e1n} = -\sin\phi \pi_n(\cos\theta) z_n(\rho) \hat{e}_\theta - \cos\phi \tau_n(cos\theta) z_n(\rho) \hat{e}_\phi, \tag{9}$$

$$M_{o1n} = \cos\phi \pi_n(\cos\theta) z_n(\rho) \hat{e}_\theta - \sin\phi \tau_n(cos\theta) z_n(\rho) \hat{e}_\phi, \tag{10}$$

$$\begin{aligned} N_{e1n} = {} & \cos\phi n(n+1) \sin\theta \pi_n(\cos\theta) \frac{z_n(\rho)}{\rho} \hat{e}_r \\ & + \cos\phi \tau_n(\cos\theta) \frac{[\rho z_n(\rho)]'}{\rho} \hat{e}_\theta - \sin\phi \pi_n(\cos\theta) \frac{[\rho z_n(\rho)]'}{\rho} \hat{e}_\phi, \end{aligned}$$

$$\begin{aligned} N_{o1n} = {} & \sin\phi n(n+1) \sin\theta \pi_n(\cos\theta) \frac{z_n(\rho)}{\rho} \hat{e}_r \\ & + \sin\phi \tau_n(\cos\theta) \frac{[\rho z_n(\rho)]'}{\rho} \hat{e}_\theta + \cos\phi \pi_n(\cos\theta) \frac{[\rho z_n(\rho)]'}{\rho} \hat{e}_\phi. \end{aligned} \tag{12}$$

The superscripts of M and N in Eqs. (4)–(7) denote the type of z_n functions in Eqs. (9)–(12) as (1) for spherical Bessel function $j_n(\rho)$, (2) for spherical Neumann function $y_n(\rho)$, and (3) for spherical Hankel function of the first kind $h_n^{(1)}(\rho)$, and $P_n^m(\cos\theta)$is the associated Legendre polynomial. The angle-dependent functions π_n and τ_n are defined in [6] as

$$\pi_n = \frac{P_n^1}{\sin\theta}, \tag{13}$$

$$\tau_n = \frac{dP_n^1}{d\theta}. \tag{14}$$

2.2. Boundary conditions

The classical motion equation for a free electron with mass m_s and charge q_s on a surface is

$$(-i\omega)m_s\vec{u}_t = q_s\vec{E}_t - \gamma_s m_s\vec{u}_t, \tag{15}$$

where γ_s is the attenuation rate from quantum physics [22], and $\vec{u}_t$ is the tangential velocity of the surface electrons, which is proportional to the tangential component of the electric field $\vec{E}_t$. The surface current density $\vec{K}$ is given by Klačka and Kocifaj [23] as

$$\vec{K} = \eta_0\vec{u}_t, \tag{16}$$

where η_0 is the static component of the surface charge density. The boundary conditions for scattering by a charged coated sphere are

$$(r=a)\begin{cases}(\vec{E}_2-\vec{E}_1)\times\hat{e}_r = 0,\\ (\vec{H}_2-\vec{H}_1)\times\hat{e}_r = \vec{K}_1 = \sigma_{s1}\vec{E}_{1t},\end{cases} \tag{17}$$

$$(r=b)\begin{cases}(\vec{E}_s+\vec{E}_i-\vec{E}_2)\times\hat{e}_r = 0,\\ (\vec{H}_s+\vec{H}_i-\vec{H}_2)\times\hat{e}_r = \vec{K}_2 = \sigma_{s2}\vec{E}_{2t},\end{cases} \tag{18}$$

with the excess charges uniformly confined to the interior or/and exterior layer surfaces. Using Eqs. (15)–(18), the surface conductivity σ_s is obtained

$$\sigma_s = \frac{e\eta_0}{(\gamma_s - i\omega)m_s}. \tag{19}$$

By incorporating Eqs. (4)–(12) into Eqs. (17)–(18), eight linear equations associated with the expansion coefficients are obtained:

$$f_n j_n(m_2x) + v_n y_n(m_2x) - c_n j_n(m_1x) = 0, \tag{20}$$

$$g_n\frac{[m_2xj_n(m_2x)]'}{m_2x} + w_n\frac{[m_2xy_n(m_2x)]'}{m_2x} - d_n\frac{[m_1xj_n(m_1x)]'}{m_1x} = 0, \tag{21}$$

$$f_n m_2\frac{[m_2xj_n(m_2x)]'}{m_2x} + v_n m_2\frac{[m_2xy_n(m_2x)]'}{m_2x} - c_n\left\{m_1\frac{[m_1xj_n(m_1x)]'}{m_1x} - \hat{g}_1 j_n(m_1x)\right\} = 0, \tag{22}$$

$$g_n m_2 j_n(m_2x) + w_n m_2 y_n(m_2x) - d_n\left\{m_1 j_n(m_1x) + \hat{g}_1\frac{[m_1xj_n(m_1x)]'}{m_1x}\right\} = 0, \tag{23}$$

$$b_n h_n^{(1)}(y) - j_n(y) + f_n j_n(m_2y) + v_n y_n(m_2y) = 0, \tag{24}$$

$$a_n\frac{\left[yh_n{}^{(1)}(y)\right]}{y} - \frac{[yj_n(y)]'}{y} + g_n\frac{[m_2yj_n(m_2y)]'}{m_2y} + w_n\frac{[m_2yy_n(m_2y)]'}{m_2y} = 0, \tag{25}$$

$$b_n\frac{\left[yh_n^{(1)}(y)\right]'}{y} - \frac{[yj_n(y)]'}{y} + f_n\left\{\frac{[m_2yj_n(m_2y)]'}{y} - \hat{g}_2 j_n(m_2y)\right\} + v_n\left\{\frac{[m_2yy_n(m_2y)]'}{y} - \hat{g}_2 y_n(m_2y)\right\} = 0, \tag{26}$$

$$a_n h_n^{(1)}(y) - j_n(y) + g_n\left\{m_2 j_n(m_2y) + \hat{g}_2\frac{[m_2yj_n(m_2y)]'}{m_2y}\right\} + w_n\left\{m_2 y_n(m_2y) + \hat{g}_2\frac{[m_2yy_n(m_2y)]'}{m_2y}\right\} = 0, \tag{27}$$

$$\hat{g} = \frac{i\omega\mu\sigma_s}{k}, \tag{28}$$

where the prime is the derivative over the argument and $\hat{g}$ represents the influence factor of the particle electrification. Nonmagnetic is assumed in this study, so that $\mu=\mu_1=\mu_2$. The arguments of the spherical Bessel functions are stated in parentheses as m_1x,m_2x,m_2y, and y, where $m_1=k_1/k$, $m_2=k_2/k$, $x=ka$ and $y=kb$. The Riccati–Bessel functions are defined as $\psi_n(\rho)=\rho j_n(\rho)$, $\xi_n(\rho)=\rho h_n^{(1)}(\rho)$ and $\chi_n(\rho)=-\rho y_n(\rho)$, which follow the Wronskian relationship $\chi_n\psi_n'-\chi_n'\psi_n=1$ [38].

2.3. Scattering coefficients

Using Eqs.Eqs. (20)–(27), the expansion coefficients of the scattering amplitudes a_n and b_n are

$$a_n = \frac{\left[(1+n\hat{g}_2/y)\tilde{D}_n/m_2 + n/y\right]\psi_n(y) - (1+\hat{g}_2\tilde{D}_n/m_2)\psi_{n-1}(y)}{\left[(1+n\hat{g}_2/y)\tilde{D}_n/m_2 + n/y\right]\xi_n(y) - (1+\hat{g}_2\tilde{D}_n/m_2)\xi_{n-1}(y)}, \tag{29}$$

$$b_n = \frac{\left[m_2\tilde{G}_n + (n/y)(1-\hat{g}_2 y/n)\right]\psi_n(y) - \psi_{n-1}(y)}{\left[m_2\tilde{G}_n + (n/y)(1-\hat{g}_2 y/n)\right]\xi_n(y) - \xi_{n-1}(y)}, \tag{30}$$

$$\tilde{D}_n = \frac{D_n(m_2 y) - A_n\chi_n'(m_2 y)/\psi_n(m_2 y)}{1 - A_n\chi_n(m_2 y)/\psi_n(m_2 y)}, \tag{31}$$

$$\tilde{G}_n = \frac{D_n(m_2 y) - B_n\chi_n'(m_2 y)/\psi_n(m_2 y)}{1 - B_n\chi_n(m_2 y)/\psi_n(m_2 y)}, \tag{32}$$

$$A_n = \psi_n(m_2 x)\frac{m_2 D_n(m_1 x) - D_n(m_2 x)\left[m_1 + \hat{g}_1 D_n(m_1 x)\right]}{m_2\chi_n(m_2 x)D_n(m_1 x) - \chi_n'(m_2 x)\left[m_1 + \hat{g}_1 D_n(m_1 x)\right]}, \tag{33}$$

$$B_n = \psi_n(m_2 x)\frac{m_2 D_n(m_2 x) - \left[m_1 D_n(m_1 x) - \hat{g}_1\right]}{m_2\chi_n'(m_2 x) - \chi_n(m_2 x)\left[m_1 D_n(m_1 x) - \hat{g}_1\right]}, \tag{34}$$

and using the definition given in [21]

$$D_n = \frac{\psi_n'}{\psi_n}, \tag{35}$$

$$\begin{cases} \hat{g}_1 = \frac{i\omega\mu\sigma_{s1}}{k} \approx \frac{x}{2}\frac{\omega_{s1}^2}{\omega^2+\gamma_{s1}^2}\left(-1 + i\frac{\gamma_{s1}}{\omega}\right), \\ \hat{g}_2 = \frac{i\omega\mu\sigma_{s2}}{k} \approx \frac{y}{2}\frac{\omega_{s2}^2}{\omega^2+\gamma_{s2}^2}\left(-1 + i\frac{\gamma_{s2}}{\omega}\right), \end{cases} \tag{36}$$

$$\begin{cases} \omega_{s1}^2 = 2\frac{e}{m_s}\frac{\Phi_1}{a^2} = \frac{N_{t1}e^2}{2\pi a^3 m_s\varepsilon_1}, \\ \omega_{s2}^2 = 2\frac{e}{m_s}\frac{\Phi_2}{b^2} = \frac{N_{t2}e^2}{2\pi b^3 m_s\varepsilon_2}, \end{cases} \tag{37}$$

$$\begin{cases} \gamma_{s1} \approx k_B T_1/\hbar, \\ \gamma_{s2} \approx k_B T_2/\hbar, \end{cases} \tag{38}$$

where ω_s is the surface plasma frequency, N_t represents the number of ions on the surface of the uniformly charged sphere, $T_{1,2}$ are the temperatures of the layers, while e and m_s are the unitary charge and mass of the electron, respectively. In addition, k_B is the Boltzmann's constant and $\hbar$ is the Planck's constant divided by the factor 2π. The derivation details for these equations are provided in Appendix A.

Considering no charge on the surfaces of the interior core and exterior shell of the coated sphere with η_{01}=η_{02}=0, then $\hat{g}_1 = \hat{g}_2 = 0$, and the coefficients in Eqs. (29)–(34) are reduced to those for a neutral coated sphere given in Bohren and Huffman [6]. If m_1=m_2, Eqs. (29)–(34) are reduced to scattering coefficients for a charged homogeneous sphere (e.g., [20]).

Using the same expressions and symbols for the amplitude scattering and scattering phase matrices as in the Lorenz-Mie theory [3,6], the elements of the scattering phase matrix are

$$\begin{cases} S_{11} = \frac{1}{2}\left(|S_1|^2 + |S_2|^2\right), \\ S_{12} = \frac{1}{2}\left(|S_2|^2 - |S_1|^2\right), \\ S_{33} = \frac{1}{2}\left(S_2^* S_1 + S_2 S_1^*\right), \\ S_{34} = \frac{1}{2}\left(S_2^* S_1 - S_2 S_1^*\right). \end{cases} \tag{39}$$

Similarly, the elements of the diagonal amplitude scattering matrix are

$$\begin{cases} S_1 = \sum\limits_n \frac{2n+1}{n(n+1)}(a_n\pi_n + b_n\tau_n), \\ S_2 = \sum\limits_n \frac{2n+1}{n(n+1)}(a_n\tau_n + b_n\pi_n), \end{cases} \tag{40}$$

and the scattering, extinction efficiencies and the asymmetry parameter$\langle\cos\Theta\rangle$[39,40] are defined as

$$\begin{cases} Q_{ext} = C_{ext}/\pi b^2 = \frac{2\pi}{k^2}\sum\limits_{n=1}^{\infty}(2n+1)\mathrm{Re}(a_n + b_n)/\pi b^2, \\ Q_{sca} = C_{sca}/\pi b^2 = \frac{2\pi}{k^2}\sum\limits_{n=1}^{\infty}(2n+1)\left(|a_n|^2 + |b_n|^2\right)/\pi b^2, \\ \langle\cos\Theta\rangle = \frac{4\pi}{k^2 C_{sca}}\mathrm{Re}\sum\limits_{n=1}^{\infty}\left[\frac{n(n+2)}{n+1}\left(a_n a_{n+1}^* + b_n b_{n+1}^*\right) + \frac{2n+1}{n(n+1)}a_n b_n^*\right]. \end{cases} \tag{41}$$

The Riccati-Bessel functions and D_n can be computed using the upward recurrence relationships given in [6]. The scattering program used for the charged coated sphere is named CHARGECOAT, and is based on the scattering program of the non-charged coated sphere BHCOAT by Bohren and Huffman [6]. The CHARGECOAT can be obtained by contacting the corresponding author.

2.4. Rayleigh approximation discussion

The radius of a sphere noticeably impacted by electrification must be significantly smaller than the wavelength, and the scattering for neutral particles with $|m|x \ll 1$ is in the Rayleigh regime [3]. The Rayleigh scattering is validated for charged particles in this section by extracting the size parameter term in the influence factor $\hat{g}$ of the particle electrification. The spherical Bessel and Neumann functions can then be expanded as a power series [27]:

$$j_n(\rho) = \frac{\rho^n}{1\cdot 3\cdot 5\cdots(2n+1)}\left[1 - \frac{\frac{1}{2}\rho^2}{1!(2n+3)} + \frac{\left(\frac{1}{2}\rho^2\right)^2}{2!(2n+3)(2n+5)} - \cdots\right], \tag{42}$$

$$y_n(\rho) = -\frac{1\cdot 3\cdot 5\cdots(2n-1)}{\rho^{n+1}}\left[1 - \frac{\frac{1}{2}\rho^2}{1!(1-2n)} + \frac{\left(\frac{1}{2}\rho^2\right)^2}{2!(1-2n)(3-2n)} - \cdots\right]. \tag{43}$$

Correspondingly, the first few terms of the Riccati–Bessel functions and their derivatives are

$$\begin{cases} \psi_1(\rho) \simeq \frac{\rho^2}{3} - \frac{\rho^4}{30}, \\ \psi_1'(\rho) \simeq \frac{2\rho}{3} - \frac{2\rho^3}{15}, \\ \chi_1(\rho) \simeq \frac{1}{\rho} + \frac{\rho}{2}, \\ \chi_1'(\rho) \simeq -\frac{1}{\rho^2} + \frac{1}{2}, \\ \xi_1(\rho) \simeq -\frac{i}{\rho} - \frac{i\rho}{2} + \frac{\rho^2}{3}, \\ \xi_1'(\rho) \simeq \frac{i}{\rho^2} - \frac{i}{2} + \frac{2\rho}{3}. \end{cases} \tag{44}$$

Considering that $\hat{g}_{1,2}$ are related to size parameters, one can define $\hat{g}_1 = \tilde{g}_1 \cdot x, \hat{g}_2 = \tilde{g}_2 \cdot y$. Using Eqs. (29)–(34), the scattering coefficients with n=1 can be simplified to the order of y^5 as

$$a = a_{c3}\cdot y^3 + a_{c4}\cdot y^4 + a_{c5}\cdot y^5 + o\left(y^6\right), \tag{45}$$

$$b = b_{c3}\cdot y^3 + b_{c4}\cdot y^4 + b_{c5}\cdot y^5 + o\left(y^6\right), \tag{46}$$

$$D = D_{cm1}{}^1\!/_y + D_{c0} + D_{c1}\cdot y + o\left(y^2\right), \tag{47}$$

$$G = G_{cm1}{}^1\!/_y + G_{c0} + G_{c1}\cdot y + o\left(y^2\right), \tag{48}$$

$$A = A_{c3}\cdot y^3 + A_{c4}\cdot y^4 + A_{c5}\cdot y^5 + o\left(y^6\right), \tag{49}$$

$$B = B_{c3}\cdot y^3 + B_{c4}\cdot y^4 + B_{c5}\cdot y^5 + o\left(y^6\right), \tag{50}$$

where

$$\begin{cases} a_{c3} = \frac{a_{u3}}{a_{d0}}, \\ a_{c4} = -\frac{a_{u3}\cdot a_{d1}}{a_{d0}^2} + \frac{a_{u4}}{a_{d0}}, \\ a_{c5} = a_{u3}\left(\frac{a_{d1}^2}{a_{d0}^3} - \frac{a_{d2}}{a_{d0}^2}\right) - \frac{a_{u4}\cdot a_{d1}}{a_{d0}^2} + \frac{a_{u5}}{a_{d0}}, \end{cases} \tag{51}$$

$$\begin{cases} a_{u3} = -\frac{2\tilde{g}_2 D_{cm1}}{3} + \frac{D_{cm1}}{3} - \frac{2m_2}{3}, \\ a_{u4} = -\frac{2\tilde{g}_2 D_{c0}}{3} + \frac{D_{c0}}{3}, \\ a_{u5} = -\frac{2\tilde{g}_2 D_{c1}}{3} + \frac{D_{c1}}{3} + \frac{2\tilde{g}_2 D_{cm1}}{15} - \frac{D_{cm1}}{30} + \frac{2m_2}{15}, \end{cases} \tag{52}$$

$$\begin{cases} a_{d0} = -i\tilde{g}_2 D_{cm1} - iD_{cm1} - im_2, \\ a_{d1} = -i\tilde{g}_2 D_{c0} - iD_{c0}, \\ a_{d2} = -i\tilde{g}_2 D_{c1} - iD_{c1} + \frac{i\tilde{g}_2 D_{cm1}}{2} - \frac{iD_{cm1}}{2} + \frac{im_2}{2}, \end{cases} \tag{53}$$

$$\begin{cases} b_{c3} = \frac{b_{u3}}{b_{d0}}, \\ b_{c4} = -\frac{b_{u3}\cdot b_{d1}}{b_{d0}^2} + \frac{b_{u4}}{b_{d0}}, \\ b_{c5} = b_{u3}\left(\frac{b_{d1}^2}{b_{d0}^3} - \frac{b_{d2}}{b_{d0}^2}\right) - \frac{b_{u4}\cdot b_{d1}}{b_{d0}^2} + \frac{b_{u5}}{b_{d0}}, \end{cases} \tag{54}$$

$$\begin{cases} b_{u3} = \frac{m_2 G_{cm1}}{3} - \frac{2}{3}, \\ b_{u4} = \frac{m_2 G_{c0}}{3}, \\ b_{u5} = -\frac{\tilde{g}_2}{3} - \frac{m_2 G_{cm1}}{30} + \frac{m_2 G_{c1}}{3} + \frac{2}{15}, \end{cases} \tag{55}$$

$$\begin{cases} b_{d0} = -im_2 G_{cm1} - i, \\ b_{d1} = -im_2 G_{c0}, \\ b_{d2} = i\tilde{g}_2 - \frac{im_2 G_{cm1}}{2} - im_2 G_{c1} + \frac{i}{2}, \end{cases} \tag{56}$$

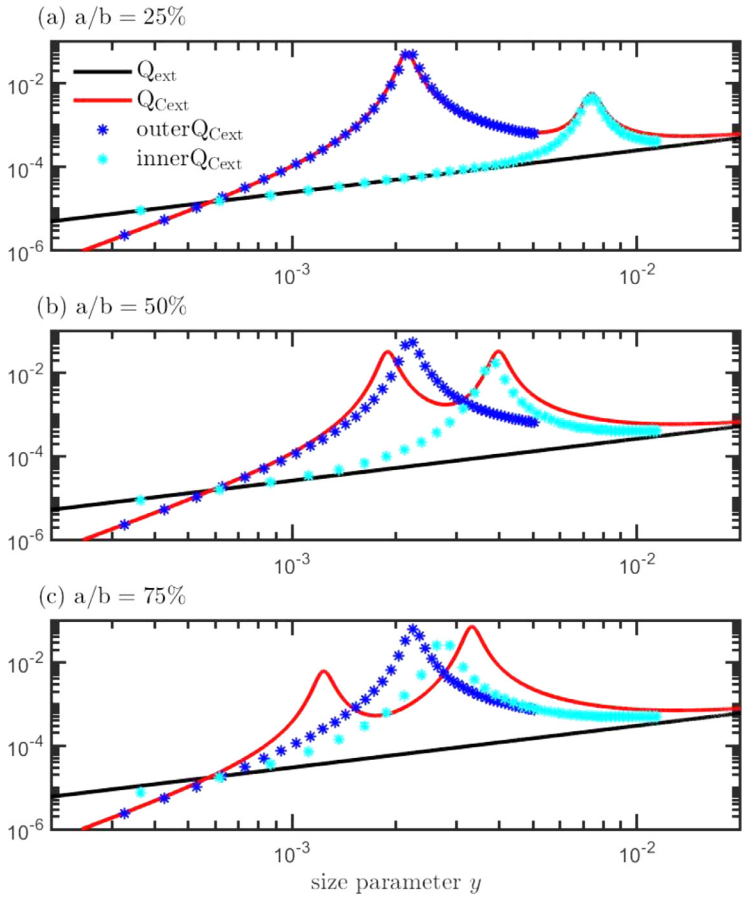

Fig. 2. Plots of the extinction efficiency for an electrically neutral coated particle with equal potential on the outer and inner surfaces. Asterisks show only charges restricted to the outer surface and only charges restricted to the inner surface, with (a)–(c) representing the results at different radii ratios.

$$\begin{cases} D_{cm1} = \frac{D_{um1}}{D_{d0}}, \\ D_{c0} = -\frac{D_{um1}\cdot D_{d1}}{D_{d0}^2} + \frac{D_{u0}}{D_{d0}}, \\ D_{c1} = D_{um1}\left(\frac{D_{d1}^2}{D_{d0}^3} - \frac{D_{d2}}{D_{d0}^2}\right) - \frac{D_{u0}\cdot D_{d1}}{D_{d0}^2} + \frac{D_{u1}}{D_{d0}}, \end{cases} \tag{57}$$

$$\begin{cases} D_{um1} = \frac{2m_2}{3} + \frac{A_{c3}r^3}{m_2^2}, \\ D_{u0} = \frac{A_{c4}r^4}{m_2^2}, \\ D_{u1} = -\frac{2m_2^3}{15} + \frac{A_{c5}r^5}{m_2^2} - \frac{A_{c3}r^3}{2}, \end{cases} \tag{58}$$

$$\begin{cases} D_{d0} = \frac{m_2^2}{3} - \frac{A_{c3}r^3}{m_2}, \\ D_{d1} = -\frac{A_{c4}r^4}{m_2}, \\ D_{d2} = -\frac{m_2^4}{30} - \frac{A_{c5}r^5}{m_2} - \frac{A_{c3}r^3 m_2}{2}, \end{cases} \tag{59}$$

$$\begin{cases} G_{cm1} = \frac{G_{um1}}{G_{d0}}, \\ G_{c0} = -\frac{G_{um1}\cdot G_{d1}}{G_{d0}^2} + \frac{G_{u0}}{G_{d0}}, \\ G_{c1} = G_{um1}\left(\frac{G_{d1}^2}{G_{d0}^3} - \frac{G_{d2}}{G_{d0}^2}\right) - \frac{G_{u0}\cdot G_{d1}}{G_{d0}^2} + \frac{G_1}{G_{d0}}, \end{cases} \tag{60}$$

$$\begin{cases} G_{um1} = -\frac{2m_2}{3}, \\ G_{u0} = -\frac{B_{c4}r^4}{m_2^2}, \\ G_{u1} = -\frac{B_{c5}r^5}{m_2^2} + \frac{2m_2^3}{15}, \end{cases} \tag{61}$$

$$\begin{cases} G_{d0} = -\frac{m_2^2}{3}, \\ G_{d1} = \frac{B_{c4}r^4}{m_2}, \\ G_{d2} = \frac{B_{c5}r^5}{m_2} + \frac{m_2^4}{30}, \end{cases} \tag{62}$$

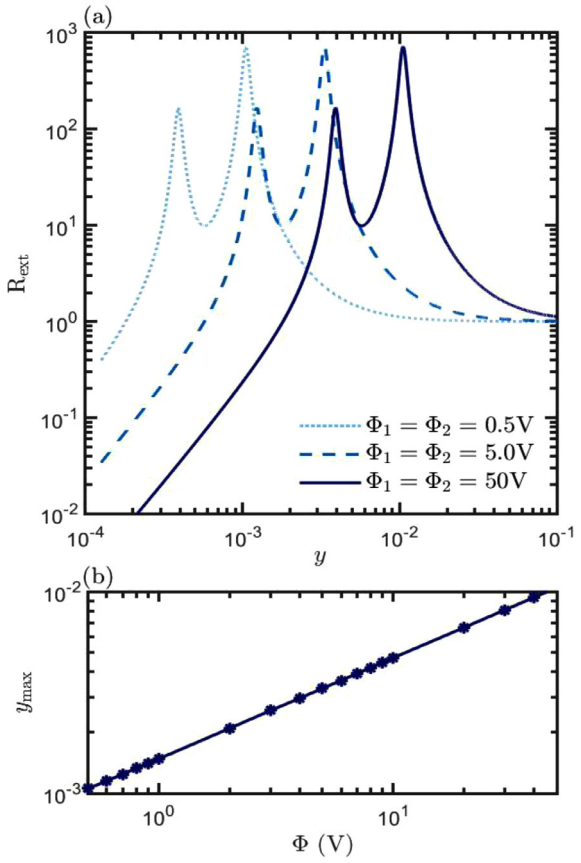

Fig. 3. (a) Changes in the R_{ext} and (b) the size parameter y_{max} corresponding to the R_{ext} peak for a charged coated particle with different surface potentials (r=75%). Other parameters are set in accordance with Fig. 2

$$\begin{cases} A_{c3} = \frac{A_{u3}}{A_{d0}}, \\ A_{c4} = -\frac{A_{u3}\cdot A_{d1}}{A_{d0}^2} + \frac{A_{u4}}{A_{d0}}, \\ A_{c5} = A_{u3}\left(\frac{A_{d1}^2}{A_{d0}^3} - \frac{A_{d2}}{A_{d0}^2}\right) - \frac{A_{u4}\cdot A_{d1}}{A_{d0}^2} + \frac{A_{u5}}{A_{d0}}, \end{cases} \tag{63}$$

$$\begin{cases} A_{u3} = 2m_2^3\left(m_1^2 - \mathrm{m}_2^2 + 2\tilde{g}_1\right), \\ A_{u4} = 0, \\ A_{u5} = -\frac{m_2^2}{5}\left(m_1^2 - \mathrm{m}_2^2 + 4\tilde{g}_1\right)\left(m_1^2 + \mathrm{m}_2^2\right), \end{cases} \tag{64}$$

$$\begin{cases} A_{d0} = -3\left(m_1^2 + 2\mathrm{m}_2^2 + 2\tilde{g}_1\right), \\ A_{d1} = 0, \\ A_{d2} = 3\tilde{g}_1\left(\frac{2}{5}m_1^2 + \mathrm{m}_2^2\right) + \frac{3}{10}\left(m_1^2 + 10\mathrm{m}_2^2\right)\left(m_1^2 - \mathrm{m}_2^2\right), \end{cases} \tag{65}$$

$$\begin{cases} B_{c3} = \frac{B_{u3}}{B_{d0}}, \\ B_{c4} = -\frac{B_{u3}\cdot B_{d1}}{B_{d0}^2} + \frac{B_{u4}}{B_{d0}}, \\ B_{c5} = B_{u3}\left(\frac{B_{d1}^2}{B_{d0}^3} - \frac{B_{d2}}{B_{d0}^2}\right) - \frac{B_{u4}\cdot B_{d1}}{B_{d0}^2} + \frac{B_{u5}}{B_{d0}}, \end{cases} \tag{66}$$

$$\begin{cases} B_{u3} = 0, \\ B_{u4} = 0, \\ B_{u5} = -\frac{m_2^2\left(m_1^2 - \mathrm{m}_2^2 + 5\tilde{g}_1\right)}{5}, \end{cases} \tag{67}$$

$$\begin{cases} B_{d0} = \frac{9}{m_2}, \\ B_{d1} = 0, \\ B_{d2} = -\frac{3\left(m_1^2 - m_2^2 + 2\tilde{g}_1\right)}{2m_2}. \end{cases} \tag{68}$$

and $a_{cn}, b_{cn}, \tilde{D}_{cn}, \tilde{G}_{cn}, A_{cn}$and B_{cn} are the n-th order coefficients in Eqs. (45)–(50), while $a_{un}, a_{dn}, b_{un}, b_{dn}, \tilde{D}_{un}, \tilde{D}_{dn}, \tilde{G}_{un}, \tilde{G}_{dn}, A_{un}, A_{dn}, B_{un}$ and B_{dn} are auxiliary functions to simplify the calculations.

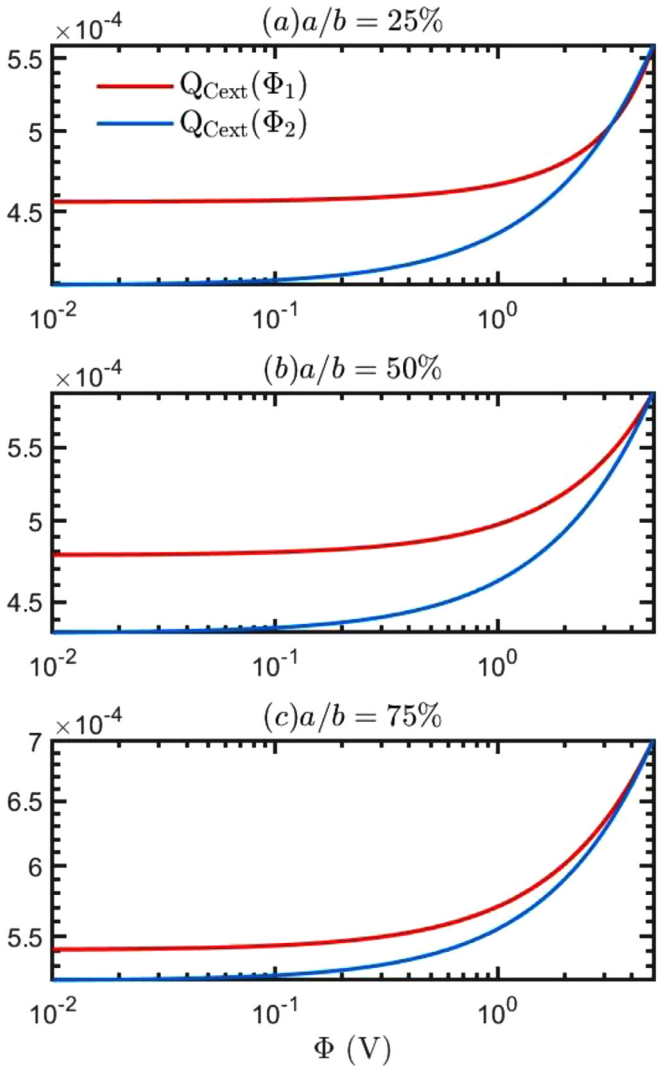

Fig. 4. Extinction efficiency for the charged coated sphere displayed as a function of the surface potential. The radius of the outer shell is 10 nm, other parameters are set in accordance with Fig. 2, with (a)–(c) representing the results at different radii ratios.

The comparison suggests that the Rayleigh scattering algorithm can replace the CHARGECOAT program when λ is approximately 2 to 3 orders of magnitude higher than the outer radius *b*.

3. Application and Discussion

Collection of electrons causes the most important effect of dust aerosol particles in the plasma environment [15]. The impact of a charged coated sphere on scattering was investigated using the CHARGECOAT program by setting both surfaces of the coated sphere with electrostatic potential of $\Phi = 5$V at a wavelength (λ) of 5.00 μm, the refractive indexes of dust-like aerosol m_1=1.25 + 0.016i and water-soluble aerosol m_2=1.45 + 0.012i [41], and temperatures $T_{1,2}$=300K.

Fig. 2 shows the effects of electrons on each surface of a charged coated sphere with respect to extinction efficiency. The arrangements are (1) electrical neutrality, (2) identical potentials on both surfaces, (3) charges only on the outer surface, and (4) charges only on the inner surface and the corresponding extinction efficiencies are denoted as Q_{ext}, Q_{Cext}, outerQ_{Cext}, and innerQ_{Cext}, respectively. The Q_{ext} represented by the black solid line gradually increases as the size parameter increases, whereas the Q_{Cext} shown by the red solid line exhibits two peaks. The differences between outerQ_{Cext} and innerQ_{Cext} relative to Q_{ext} are exhibited by the dark blue and light blue asterisks, respectively. The outerQ_{Cext} peak occurs at $y \approx 2\times10^{-3}$, and obviously remains unchanged as the radius ratio varies. However, as the ratio increases, the extinction peak of the innerQ_{Cext} caused by the charges on the inner surface tend to increase and shift toward a lower size parameter, as thickly coated particles weaken the influence of electrons on the surface of the core. As the shell becomes thinner, the inner peak increases and moves closer to the outer surface peak. For particles with both surfaces charged, the Q_{Cext} shows good agreement with the innerQ_{Cext} and outerQ_{Cext} peaks in Fig. 2(a). Nevertheless, the curve for a thinly-coated particle exhibits a smaller peak relative to that for the outerQ_{Cext}. The electrification effect contains the interaction of the coated sphere and is not completely superimposed by the effect of the two charged surfaces.

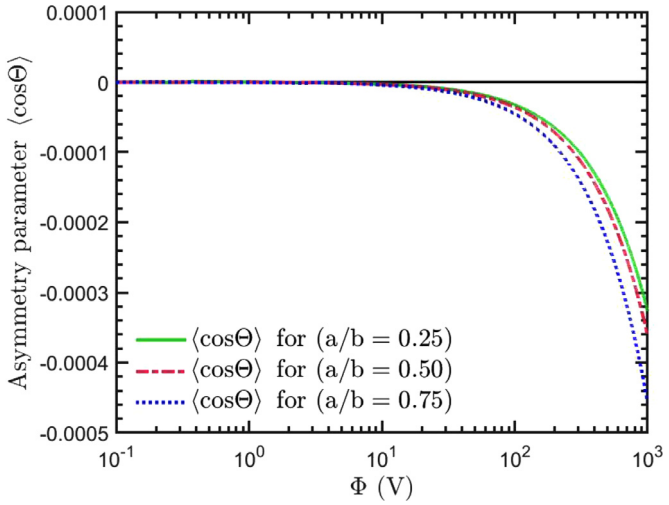

Fig. 5. Asymmetry parameters of charged coated spheres as the function of surface potential. The size parameter of the outer shell y is 0.001 and $\Phi_1 = \Phi_2$, other parameters are set in accordance with Fig. 2(a). The black line represents $\langle \cos \Theta \rangle = 0$.

The extinction efficiency differences between charged and electrically neutral coated spheres are displayed by two solid lines. As the size parameter increases, the Q_{Cext} attain two peaks, and then declines steadily. According to the asterisks, the outer surface peak is associated with a smaller size parameter. The two peaks also involve different oscillations, with that on the left being dominated by the charges on the surface of the exterior shell while that on the right is mainly observed due to charges on the interior core surface. The influence of the surface charges on the optical properties is negligible when $y \geq 2 \times 10^{-2}$. Along with the growth of $r = a/b$, the size parameter y_{max} linked with the maximum Q_{max} apparently shifted to the left, with the right peak increasing and that attributed to exterior surface charges decreasing. At $r = 25\%$, the peaks associated with the surface charges of the exterior layer are prominent, and Q_{Cext} is approximately 1000 times as large as Q_{ext} with $y \approx 7\times10^{-4}$, i.e., the extinction ratio R_{ext}=Q_{Cext}/Q_{ext} reaches about 1000, whereas the extinction peak caused by charges on the interior layer surface $\{innerQ_{Cext}\}_{max}$ reaches a maximum when $r = 75\%$. The results show that the dominant peak value is related to the fraction ratio of the core-shell structure.

According to the features in Fig. 3, the extinction efficiency ratios $R_{ext} = Q_{Cext}/Q_{ext}$ exhibit similar characteristics at different potentials. The size parameter y_{max} corresponding to the R_{ext} peak is proportional to the potentials on the surface, as demonstrated by the monotonic increase in Fig. 3(b).

Fig. 4 shows the variation of charged extinction efficiency with surface potential when the other surface is held at 5V. The extinction efficiency of the charged outer shell has a more pronounced tendency with potential, while the effect of the inner charges is attenuated by the spherical shell. As the ratio of radii increases, the difference caused by the charges on the inner and outer surfaces decreases.

The scattering phase matrix of a charged coated sphere are the same as that of Rayleigh scattering according to section 2.4. Fig. 5 shows the asymmetry parameters associated with different radius ratios as a function of surface potential. The parameters are set according to Fig. 2(a), except for $y = 0.001$ and Φ_1=Φ_2. Asymmetry parameter indicates the tendency of scattering distribution as 0 for symmetric, positive for forward-wise, and negative for backward-wise scatterings. On the one hand, the asymmetry parameters begin to deviate from zero with the increased surface potential, but on the other hand, the asymmetry parameter values are still less than $5e^{-4}$ with the surface potentials up to 1000V. The results show that the appropriate amount of charges cannot cause significant deviations to Rayleigh scattering, which further confirms the validation of the Rayleigh approximation in section 2.4.

4. Conclusion

An analytical solution for scattering by electrically charged coated spheres was derived using the Lorenz–Mie theory in this study. The solution was generalized for scattering by a coated sphere with uniformly distributed surface charges. Correspondingly, the CHARGECOAT program was suitable for scattering by a coated sphere with or without charges on one or both the surfaces and for scattering by a homogeneous sphere with or without charges on the surface. The charges on both surfaces of a coated sphere can be different, and input charges can be stated as charge amount, surface potential or conductivity. Rayleigh scattering was also derived in detail using the Taylor expansion for scattering of a charged coated sphere in the Rayleigh regime. Charges on different surfaces of a core-shell structure sphere produced two peaks for the efficiency factor, which were related to the radius ratio. Charged coated spheres with thick shells weakened the influence of charges on the inner surface, while the overall efficiencies of the thin shell charged coated spheres were mainly influenced by the charged interior layer.

At any specified temperature and wavelength, the maximum extinction value can be magnified by one to three orders of magnitude, and is mainly affected by the following parameters: 1) the radius ratio of the inner core and outer coating and 2) the amounts of electrons on the surfaces. As the inner radius increased, the extinction peak dominated by the surface charges on the interior core also increased, and the peaks shifted toward the lower size parameters. Moreover, for a thick coating sphere the extinction efficiency peaks corresponding to the surface charges of the interior core and the exterior coating were consistent with the respective peaks for coated spheres with only core or coating charged. Since the extinction efficiency that was amplified by charges mainly occurred in the Rayleigh regime and the scattering distribution displayed Rayleigh scattering characteristics, Rayleigh scattering given inEqs. (45)–(68) is adequate to represent the analytical solution obtained using the Lorenz–Mie theory.

Declaration of Competing Interest

The authors declare that they have no known competing financial interests or personal relationships that could have appeared to influence the work reported in this paper.

Acknowledgments

The authors are grateful to Drs. Bohren and Huffman for use of their BHCOAT code. Bingqiang Sun acknowledges support from the Natural Science Foundation of Shanghai (Grant No. 19ZR1404100) and the National Natural Science Foundation of China (Grant No. 41975021). Yijung Zhang also acknowledges the support of the National Natural Science Foundation of China (Grant No. 41875001).

APPENDIX A: Derivation process

After substituting the Riccati-Bessel functions into the expansion coefficients, Eqs. (20)–(27) are transformed to the following equations:

$$f_n m_1 \psi_n(m_2 x) - v_n m_1 \chi_n(m_2 x) - c_n m_2 \psi_n(m_1 x) = 0, \tag{A1}$$

$$-g_n m_1 \psi_n'(m_2 x) + w_n m_1 \chi_n'(m_2 x) + d_n m_2 \psi_n'(m_1 x) = 0, \tag{A2}$$

$$f_n m_1 \psi_n'(m_2 x) - v_n m_1 \chi_n'(m_2 x) - c_n\left[m_1 \psi_n'(m_1 x) - \hat{g}_1 \psi_n(m_1 x)\right] = 0, \tag{A3}$$

$$-g_n m_1 \psi_n(m_2 x) + w_n m_1 \chi_n(m_2 x) + d_n\left[m_1 \psi_n(m_1 x) + \hat{g}_1 \psi'_n(m_1 x)\right] = 0, \tag{A4}$$

$$b_n m_2 \xi_n(y) - m_2 \psi_n(y) + f_n \psi_n(m_2 y) - v_n \chi_n(m_2 y) = 0, \tag{A5}$$

$$a_n m_2 \xi_n'(y) - m_2 \psi_n'(y) + g_n \psi_n'(m_2 y) - w_n \chi_n'(m_2 y) = 0, \tag{A6}$$

$$b_n m_2 \xi_n'(y) - m_2 \psi_n'(y) + f_n\left[m_2 \psi_n'(m_2 y) - \hat{g}_2 \psi_n(m_2 y)\right] - v_n\left[m_2 \chi_n'(m_2 y) - \hat{g}_2 \chi_n(m_2 y)\right] = 0, \tag{A7}$$

$$a_n m_2 \xi_n(y) - m_2 \psi_n(y) + g_n\left[m_2 \psi_n(m_2 y) + \hat{g}_2 \psi_n'(m_2 y)\right] - w_n\left[m_2 \chi_n(m_2 y) + \hat{g}_2 \chi_n'(m_2 y)\right] = 0. \tag{A8}$$

Eliminating d_n in Eq. (A2) and (A4), and defining $A_n = w_n/g_n$, one can obtain

$$\begin{aligned} A_n = \frac{w_n}{g_n} &= \frac{m_1 \psi_n(m_1 x)\psi_n'(m_2 x) + \hat{g}_1 \psi_n'(m_1 x)\psi_n'(m_2 x) - m_2 \psi_n'(m_1 x)\psi_n(m_2 x)}{m_1 \psi_n(m_1 x)\chi_n'(m_2 x) + \hat{g}_1 \psi_n'(m_1 x)\chi_n'(m_2 x) - m_2 \psi_n'(m_1 x)\chi_n(m_2 x)} \\ &= \psi_n(m_2 x)\frac{m_2 D_n(m_1 x) - D_n(m_2 x)\left[m_1 + \hat{g}_1 D_n(m_1 x)\right]}{m_2 D_n(m_1 x)\chi_n(m_2 x) - \chi_n'(m_2 x)\left[m_1 + \hat{g}_1 D_n(m_1 x)\right]}. \end{aligned} \tag{A9}$$

By eliminating w_n and g_n in Eq. (A6) and (A8), respectively, a_n can be expressed using g_n and w_n as

$$g_n = \frac{a_n\left[m_2 \xi_n'(y)\chi_n(m_2 y) + \hat{g}_2 \xi_n'(y)\chi_n'(m_2 y) - \xi_n(y)\chi_n'(m_2 y)\right] - \left[m_2 \psi_n'(y)\chi_n(m_2 y) + \hat{g}_2 \psi_n'(y)\chi_n'(m_2 y) - \psi_n(y)\chi_n'(m_2 y)\right]}{\chi_n'(m_2 y)\psi_n(m_2 y) - \psi_n'(m_2 y)\chi_n(m_2 y)}, \tag{A10}$$

$$w_n = \frac{a_n\left[m_2 \xi_n'(y)\psi_n(m_2 y) + \hat{g}_2 \xi_n'(y)\psi_n'(m_2 y) - \xi_n(y)\psi_n'(m_2 y)\right] - \left[m_2 \psi_n'(y)\psi_n(m_2 y) + \hat{g}_2 \psi_n'(y)\psi_n'(m_2 y) - \psi_n(y)\psi_n'(m_2 y)\right]}{\chi_n'(m_2 y)\psi_n(m_2 y) - \psi_n'(m_2 y)\chi_n(m_2 y)}, \tag{A11}$$

$$\begin{aligned} a_n &= \frac{A_n\left[m_2 \psi_n'(y)\chi_n(m_2 y) + \hat{g}_2 \psi_n'(y)\chi_n'(m_2 y) - \psi_n(y)\chi_n'(m_2 y)\right] - \left[m_2 \psi_n'(y)\psi_n(m_2 y) + \hat{g}_2 \psi_n'(y)\psi_n'(m_2 y) - \psi_n(y)\psi_n'(m_2 y)\right]}{A_n\left[m_2 \xi_n'(y)\chi_n(m_2 y) + \hat{g}_2 \xi_n'(y)\chi_n'(m_2 y) - \xi_n(y)\chi_n'(m_2 y)\right] - \left[m_2 \xi_n'(y)\psi_n(m_2 y) + \hat{g}_2 \xi_n'(y)\psi_n'(m_2 y) - \xi_n(y)\psi_n'(m_2 y)\right]} \\ &= \frac{\psi_n(y)\left[\left(1 + \hat{g}_2 \frac{n}{y}\right)\tilde{D}_n/m_2 + \frac{n}{y}\right] - \psi_{n-1}(y)\left(1 + \hat{g}_2 \tilde{D}_n/m_2\right)}{\xi_n(y)\left[\left(1 + \hat{g}_2 \frac{n}{y}\right)\tilde{D}_n/m_2 + \frac{n}{y}\right] - \xi_{n-1}(y)\left(1 + \hat{g}_2 \tilde{D}_n/m_2\right)}. \end{aligned} \tag{A12}$$

Similarly, b_n can be expressed as

$$\begin{aligned} B_n = \frac{v_n}{f_n} &= \frac{m_1 \psi_n'(m_1 x)\psi_n(m_2 x) - \hat{g}_1 \psi_n(m_1 x)\psi_n(m_2 x) - m_2 \psi_n(m_1 x)\psi_n'(m_2 x)}{m_1 \psi_n'(m_1 x)\chi_n(m_2 x) - \hat{g}_1 \psi_n(m_1 x)\chi_n(m_2 x) - m_2 \psi_n(m_1 x)\chi_n'(m_2 x)} \\ &= \psi_n(m_2 x)\frac{m_2 D_n(m_2 x) - \left[m_1 D_n(m_1 x) - \hat{g}_1\right]}{m_2 \chi_n'(m_2 x) - \chi_n(m_2 x)\left[m_1 D_n(m_1 x) - \hat{g}_1\right]}, \end{aligned} \tag{A13}$$

$$f_n = \frac{b_n\left[m_2 \xi_n(y)\chi_n'(m_2 y) - \hat{g}_2 \xi_n(y)\chi_n(m_2 y) - \xi_n'(y)\chi_n(m_2 y)\right] - \left[m_2 \psi_n(y)\chi_n'(m_2 y) - \hat{g}_2 \psi_n(y)\chi_n(m_2 y) - \psi_n'(y)\chi_n(m_2 y)\right]}{\chi_n(m_2 y)\psi_n'(m_2 y) - \chi_n'(m_2 y)\psi_n(m_2 y)}, \tag{A14}$$

$$v_n = \frac{b_n\left[m_2 \xi_n(y)\psi_n'(m_2 y) - \hat{g}_2 \xi_n(y)\psi_n(m_2 y) - \xi_n'(y)\psi_n(m_2 y)\right] - \left[m_2 \psi_n(y)\psi_n'(m_2 y) - \hat{g}_2 \psi_n(y)\psi_n(m_2 y) - \psi_n'(y)\psi_n(m_2 y)\right]}{\chi_n(m_2 y)\psi_n'(m_2 y) - \chi_n'(m_2 y)\psi_n(m_2 y)}, \tag{A15}$$

$$\begin{aligned} b_n &= \frac{B_n\left[m_2 \psi_n(y)\chi_n'(m_2 y) - \hat{g}_2 \psi_n(y)\chi_n(m_2 y) - \psi_n'(y)\chi_n(m_2 y)\right] - \left[m_2 \psi_n(y)\psi_n'(m_2 y) - \hat{g}_2 \psi_n(y)\psi_n(m_2 y) - \psi_n'(y)\psi_n(m_2 y)\right]}{B_n\left[m_2 \xi_n(y)\chi_n'(m_2 y) - \hat{g}_2 \xi_n(y)\chi_n(m_2 y) - \xi_n'(y)\chi_n(m_2 y)\right] - \left[m_2 \xi_n(y)\psi_n'(m_2 y) - \hat{g}_2 \xi_n(y)\psi_n(m_2 y) - \xi_n'(y)\psi_n(m_2 y)\right]} \\ &= \frac{\psi_n(y)\left(m_2 \tilde{G}_n - \hat{g}_2 + \frac{n}{y}\right) - \psi_{n-1}(y)}{\xi_n(y)\left(m_2 \tilde{G}_n - \hat{g}_2 + \frac{n}{y}\right) - \xi_{n-1}(y)}. \end{aligned} \tag{A16}$$

Eventually, Eqs. (29)–(34) are obtained and organized for the computations.

References

[1] Lorenz LV. Upon the light reflected and refracted by a transparent sphere. Vidensk. Selsk. Shrifter 1890;6:1–62.
[2] Mie Gustav. Beiträge zur Optik trüber Medien, speziell kolloidaler Metallösungen. Ann Phys 1908;330:377–445.
[3] van de Hulst HC. Light Scattering by Small Particles. New York: Wiley; 1981.
[4] Wiscombe WJ. Improved Mie scattering algorithms. Appl Opt 1980;19:1505–9.
[5] Aden AL, Kerker M. Scattering of Electromagnetic Waves from Two Concentric Spheres. J Appl Phys 1951;22:1242–6.
[6] Bohren CF, Huffman DR. Absorption and Scattering of Light by Small Particles. John Wiley & Sons; 2004.
[7] Bhandari R. Scattering coefficients for a multilayered sphere: analytic expressions and algorithms. Appl Opt 1985;24:1960–7.
[8] Bonnet RM, Blanc M. Planetary atmospheric electricity. Springer Science & Business Media; 2008.
[9] Loeb LB. Static electrification. Springer Science & Business Media; 2012.
[10] G. Videen, M. Kocifaj, and J. Klačka, "Method and apparatus for lightning threat indication," US10859694B2.
[11] Kocifaj M, Videen G, Klačka J. Backscatter in a cloudy atmosphere as a lightning-threat indicator. J. Quant. Spectrosc. Radiat. Transf 2015;150:175–80.
[12] Takahashi T, Sugimoto S, Kawano T, Suzuki K. Riming Electrification in Hokuriku Winter Clouds and Comparison with Laboratory Observations. J Atmos Sci 2017;74:431–47.
[13] Takahashi T, Tajiri T, Sonoi Y. Charges on Graupel and Snow Crystals and the Electrical Structure of Winter Thunderstorms. J Atmos Sci 1999;56:1561–78.
[14] Takahashi T. Riming Electrification as a Charge Generation Mechanism in Thunderstorms. J Atmos Sci 1978;35:1536–48.
[15] Thiessen E, Heinisch RL, Bronold FX, Fehske H. Infrared light extinction by charged dielectric core-coat particles. Eur Phys J D 2014;68:98.
[16] Pahtz T, Herrmann HJ, Shinbrot T. Why do particle clouds generate electric charges? Nat Phys 2010;6:364–8.
[17] Takahashi T. Thunderstorm Electrification-A Numerical Study. J Atmos Sci 1984;41:2541–58.
[18] Saunders C. Charge Separation Mechanisms in Clouds. Space Sci Rev 2008;137:335–53.
[19] Latham J, Mason BJ. Electric charge transfer associated with temperature gradients in ice. Proc. Royal Society Series A 1961;260:523–36.
[20] Bohren CF, Hunt AJ. Scattering of electromagnetic waves by a charged sphere. Can J Phys 1977;55(21):1930–5.
[21] Klačka J, Kocifaj M. Scattering of electromagnetic waves by charged spheres and some physical consequences. J. Quant. Spectrosc. Radiat. Transf. 2007;106:170–83.
[22] Klačka J, Kocifaj M. On the scattering of electromagnetic waves by a charged sphere. Prog. Electromagn. Res. 2010;109:17–35.
[23] Klačka J, Kocifaj M, Kundracik F, Videen G. Optical signatures of electrically charged particles: Fundamental problems and solutions. J. Quant. Spectrosc. Radiat. Transf. 2015;164:45–53.
[24] Klačka J, Kocifaj M, Kundracik F, Videen G, Kohut I. Generalization of electromagnetic scattering by charged grains through incorporation of interband and intraband effects. Opt Lett 2015;40:5070–3.
[25] Zhou Z, Zhang S, Qi J, Yang X. Extension of complex refractive index model and analysis of scattering properties of charged submicron spheres. J. Quant. Spectrosc. Radiat. Transf. 2020;242:106735.
[26] Rosenkrantz E, Arnon S. Enhanced absorption of light by charged nanoparticles. Opt Lett 2010;35:1178.
[27] Strutt JW. On the light from the sky, its polarization and colour. Philos Mag 1871;41:107–20 and 274-279.
[28] He Q, Zhou Y, Zheng X. Effects of charged sand on electromagnetic wave propagation and its scattering field. Science in China Series G 2006;49:77–87.
[29] Li X, Xie L, Zheng X. The comparison between the Mie theory and the Rayleigh approximation to calculate the EM scattering by partially charged sand. J. Quant. Spectrosc. Radiat. Transf. 2012;113:251–8.
[30] Massling A, Stock M, Wiedensohler A. Diurnal, weekly, and seasonal variation of hygroscopic properties of submicrometer urban aerosol particles. Atmospheric Environ 2005;39:3911–22.
[31] Johnson BR. Light scattering by a multilayer sphere. Appl Opt 1996;35:3286–96.
[32] Fuller KA. Scattering of light by coated spheres. Opt Lett 1993;18:257–9.
[33] Wu ZS, Wang YP. Electromagnetic scattering for multilayered sphere: Recursive algorithms. Radio Sci 1991;26:1393–401.
[34] Xingcai L, Beidou Z. An equivalent solution for the electromagnetic scattering of multilayer particle. J. Quant. Spectrosc. Radiat. Transf. 2013;129:236–40.
[35] Zhifang S, Zhenya L. Equivalent dielectric constant of inhomogeneous dielectric spherical particle. College Physics 2005;2.
[36] Kundracik F, Kocifaj M, Videen G, Markoš P. Optical properties of charged nonspherical particles determined using the discrete dipole approximation. J. Quant. Spectrosc. Radiat. Transf. 2020;254:107245.
[37] Li X, Zhang B. The electromagnetic scattering of the charged inhomogeneous sand particle. J. Quant. Spectrosc. Radiat. Transf. 2013;119:150–4.
[38] Abramowitz M, Stegun IA. Handbook of Mathematical Functions with Formulas, Graphs, and Mathematical Tables. J. Am. Stat. Assoc. 1966;59:1324.
[39] Sun B, Bi L, Yang P, Kahnert M, Kattawar G. Invariant Imbedding T-matrix method for light scattering by nonspherical and inhomogeneous particles. Elsevier; 2019.
[40] Mishchenko MI, Travis LD, Lacis AA. Scattering, absorption, and emission of light by small particles. Cambridge University Press; 2002.
[41] World Meteorological OrganizationA Preliminary Cloudless Standard Atmosphere for Radiation Computation. World Climate Programme 2021 WMO/TD-No 24WCP- No 1121986.